REFERENCES AND NOTES

1. P. Yager and P. Schoen, *Mol. Cryst. Liq. Cryst.* **106**, 371 (1984).
2. _____, C. Davies, R. Price, A. Singh, *Biophys. J.* **48**, 899 (1985).
3. For a recent review, see J. M. Schnur, *Science* **262**, 1669 (1993).
4. D. D. Archibald and S. Mann, *Nature* **364**, 430 (1993).
5. R. Dagani, *Chem. Eng. News* **71**, 19 (9 August 1993).
6. B. N. Thomas *et al.*, *Mater. Res. Soc. Symp. Proc.* **248**, 83 (1992).
7. M. Caffrey, J. Hogan, A. S. Rudolph, *Biochemistry* **30**, 2134 (1991).
8. B. Ratna *et al.*, *Chem. Phys. Lipids* **63**, 47 (1992).
9. The in vacuo conditions required for electron microscopy may exaggerate the measured tubule diameter as a result of flattening upon interlamellar solvent evaporation. The upper limit of distortion for a completely collapsed, infinitely elastic monolamellar tubule is the factor of $(\pi D)/2$, where D is the hydrated tubule diameter.
10. See, for example, S. Nir, J. Bentz, J. Wilschut, N. Duzgunes, *Prog. Surf. Sci.* **13**, 1 (1983). DPPC, DSPC, and DMPC are dipalmitoylphosphatidylcholine, distearoylphosphatidycholine, and dimyristoylphosphatidylcholine, respectively.
11. V. Luzzati, *Biol. Membr.* **1**, 71 (1968).
12. A. Tardieu *et al.*, *J. Mol. Biol.* **75**, 711 (1973).
13. M. J. Janiak, D. M. Smalley, G. G. Shipley, *J. Biol. Chem.* **254**, 6068 (1979).
14. G. S. Smith, E. B. Sirota, C. R. Safinya, N. A. Clark, *Phys. Rev. Lett.* **60**, 813 (1988).
15. E. B. Sirota *et al.*, *Science* **242**, 1406 (1988).
16. G. S. Smith, E. B. Sirota, C. R. Safinya, R. J. Plano, N. A. Clark, *J. Chem. Phys.* **92**, 4519 (1990).
17. C. R. Safinya *et al.*, *Phys. Rev. Lett.* **57**, 2718 (1986); D. Roux and C. R. Safinya, *J. Phys. (Paris)* **49**, 307 (1988).
18. P. G. De Gennes, *C. R. Acad. Sci.* **304**, 259 (1987).
19. T. C. Lubensky and J. Prost, *J. Phys. II (Paris)* **2**, 371 (1992).
20. W. Helfrich and J. Prost, *Phys. Rev. A* **38**, 3065, (1988).
21. Z.-C. Ou-Yang and L.-X. Liu, *Phys. Rev. Lett.* **65**, 1679 (1990); *Phys. Rev. A* **43**, 6826 (1991).
22. J. V. Selinger and J. M. Schnur, *Phys. Rev. Lett.* **71**, 4091 (1993).

23. We gratefully acknowledge useful conversations with R. Shashidar, B. Ratna, E. B. Sirota, and P. Pincus. We thank R. Shashidar for providing the phospholipid. Portions of this work were executed at beamlines X10A and X10B of the National Synchrotron Light Source at Brookhaven National Laboratory, administered by the Department of Energy. B.N.T. and N.A.C. were supported in part by National Science Foundation (NSF) grant DMR 92-23729 to N.A.C. C.R.S. was supported in part by NSF grants DMR-92-21742 and DMR-93-01199 and the Petroleum Research Fund (grant 27837-AC7). B.N.T. thanks the Exxon Research and Engineering Company for their generous extension of office space, x-ray facilities, microscopy, and computing equipment.

12 October 1994; accepted 19 January 1995

Crystal Structure and Function of the Isoniazid Target of *Mycobacterium tuberculosis*

Andréa Dessen,* Annaïk Quémard,* John S. Blanchard,† William R. Jacobs Jr., James C. Sacchettini†

Resistance to isoniazid in *Mycobacterium tuberculosis* can be mediated by substitution of alanine for serine 94 in the InhA protein, the drug's primary target. InhA was shown to catalyze the β-nicotinamide adenine dinucleotide (NADH)–specific reduction of 2-*trans*-enoyl–acyl carrier protein, an essential step in fatty acid elongation. Kinetic analyses suggested that isoniazid resistance is due to a decreased affinity of the mutant protein for NADH. The three-dimensional structures of wild-type and mutant InhA, refined to 2.2 and 2.7 angstroms, respectively, revealed that drug resistance is directly related to a perturbation in the hydrogen-bonding network that stabilizes NADH binding.

Isoniazid has been a first-line chemotherapeutic in the treatment of tuberculosis since 1952 (*1*) but is ineffective against newly emergent strains of *Mycobacterium tuberculosis* that have shown themselves to be drug-resistant. Such strains cause mortality in 70 to 90% of AIDS-stricken patients who develop tuberculosis (*2*). Isoniazid is believed to kill mycobacteria by inhibiting the biosynthesis of mycolic acids—long-chain α-branched β-hydroxy fatty acids that are critical components of the mycobacterial cell wall (*3*). In 25 to 50% of isoniazid-resistant strains, drug resistance is associated with a loss of catalase and peroxidase activities, both of which are encoded by the *katG* gene (*4*, *5*). These activities are thought to participate in the drug sensitivity mechanism by converting isoniazid in vivo into its biologically active form, which then acts on its intracellular target (*6*).

Genetic studies have identified the protein product of the *inhA* gene as the primary target for the action of isoniazid and ethionamide, a closely related chemical analog. Notably, 20 to 25% of isoniazid-resistant clinical isolates display mutations in the *inhA* locus, and substitutions within the *inhA* open reading frame have been shown to express the $Ser^{94} \rightarrow Ala^{94}$ (S94A) and $Ile^{16} \rightarrow Thr^{16}$ (I16T) InhA enzymes (*5*, *7*, *8*).

InhA from *M. tuberculosis* displays 32% amino acid identity with enoyl–acyl carrier protein (ACP) reductase of *Brassica napus* and 40% identity with EnvM from *Escherichia coli* (*5*, *7*–*9*). EnvM is the target of a group of antibacterial compounds, the diazaborines (*9*, *10*), and has been shown to catalyze the reduction of crotonoyl-ACP (*11*). A $Gly^{93} \rightarrow Ser^{93}$ mutation in EnvM, which maps four amino acids from Ser^{94} in the corresponding InhA sequence (*7*), leads to a diazaborine-resistant phenotype (*10*). Thus, Gly^{93} (EnvM) and Ser^{94} (InhA) may lie in analogous regions of the proteins, and the drug resistance mechanisms may share some similarities. A mechanism for diazaborine inhibition of EnvM has recently been proposed (*11*). Here we describe biochemical and structural features of InhA that provide insight into the molecular mechanism of isoniazid resistance.

To determine the biochemical properties of InhA, we subcloned the *inhA* gene into a T7-based vector, overexpressed the protein product in *E. coli*, and purified the product by classic protein purification methods done at 4°C. The purity and size of recombinant InhA were determined by liquid chromatography–electrospray mass spectrometry (LC-MS) (*12*). By following the oxidation of NADH by means of a spectrophotometric assay, we showed that InhA catalyzed the reduction of 2-*trans*-octenoyl-ACP, thus identifying the *inhA* gene product as an enoyl-ACP reductase (Table 1). This result is consistent with the suggestion that InhA participates in mycolic acid biosynthesis (*7*). Enoyl-ACP reduction was linearly dependent on the concentration of added InhA. The kinetic values for InhA were similar to steady-state Michaelis constants for NADH and crotonoyl-ACP exhibited by the *B. napus* enoyl-ACP reductase (*13*). Neither isoniazid nor ethionamide bound to InhA, as assessed by titration microcalorimetry (*14*), which suggests that the drugs must be activated before binding.

We also expressed and purified the S94A form of InhA in an identical manner to that used for the wild-type protein. Kinetic evaluation of the S94A InhA-catalyzed reduction of 2-*trans*-octenoyl-ACP by NADH revealed that the values for the K_m and V_{max} of the enoyl substrate did not differ significantly from the wild-type values; however, the Michaelis constant for NADH was five times higher in the S94A mutant (Table 1). This observation suggested that the mechanism of drug resistance may be related to specific interactions between enzyme and cofactor within the NADH binding site.

To explore the structural basis of this difference, we prepared crystals of recombinant wild-type and S94A InhA in the pres-

A. Dessen, J. S. Blanchard, J. C. Sacchettini, Department of Biochemistry, Albert Einstein College of Medicine, 1300 Morris Park Avenue, Bronx, NY 10461, USA. A. Quémard and W. R. Jacobs Jr., Departments of Microbiology and Immunology and Howard Hughes Medical Institute, Albert Einstein College of Medicine, Bronx, NY 10461, USA.

*These authors contributed equally to this work.
†To whom correspondence should be addressed.

ence of NADH. Crystals for both wild type and mutant were hexagonal, space group $P6_222$, with unit cell dimensions of $a = b = 100.14$ Å, $c = 140.45$ Å, and $\alpha = \beta = 90°$, $\gamma = 120°$, with one molecule per asymmetric unit. The solvent content of the crystals was ~60%. The crystal structures were solved by multiple isomorphous replacement (MIR) methods with the use of two heavy-atom derivatives (*15*, *16*). The wild-type structure was refined to 2.2 Å and the structure of S94A to 2.7 Å (Table 2).

The polypeptide backbone of the InhA subunit folds into a single structural domain of 42 × 52 × 40 Å (Fig. 1). Overall, the enzyme structure has a "chairlike" appearance and is composed of seven β strands (B1 through B7) and eight α helices (A1 through A8). The core structure (the "legs" and "seat") is topologically similar to the dinucleotide-binding fold of many dehydrogenases (*17*). The cofactor binding site is a shallow pocket between the back and the seat of the InhA structure. NADH lies in an extended conformation in the pocket, along the top of the COOH-termini of the core β sheet (with the exception of B4 and B5, whose COOH-termini extend beyond NADH) (Fig. 1). The adenine ring is parallel to the seat of InhA, and the nicotinamide portion of NADH faces the back, pointing deep into a cavity formed by β strands B4, B5, and B6 and by α helices A5, A6, and A7. Because this cavity is composed primarily of aromatic and hydrophobic side chains, we propose that it makes up the lipid binding site in enoyl-ACP reductase.

The structure of the NADH binding site of InhA suggests that recognition of NADH is mediated by interactions with an array of polar amino acids and backbone atoms. The nucleotide forms hydrogen bonds with Asp^{64} (OD2 → N6A), Ser^{20} (OG → O2PA), and Lys^{165} (NZ → O2′N), as well as the main-chain oxygen and nitrogen atoms of Val^{65} (N → N1A), Gly^{14} (O → O3′A), Ile^{194} (N → O7N), Ile^{21} (N → O2PN), and six water molecules within the pocket. The pyrophosphate moiety of NADH is near the loop connecting B1 to A1. Although the geometries of the active sites and the position of NADH in the wild-type and mutant enzymes are very similar, a striking difference is found in the position of the backbone atoms of Gly^{14}, the first residue in loop 1. In the wild-type structure, O2 of the P_N phosphate of NADH forms hydrogen bonds with the main-chain nitrogen atom of Ile^{21} and a well-ordered water molecule. This water molecule, in turn, hydrogen bonds to the hydroxyl group of Ser^{94}, the main-chain oxygen of Gly^{14}, and the main-chain nitrogen atoms of Ala^{22} and Ile^{21} (Fig. 2A). In the S94A mutant, however, the carbonyl group of Gly^{14} faces away from the nucleotide, disrupting the hydrogen bond made with the water molecule in the wild-type structure (Fig. 2B). In S94A this water molecule is disordered, as indicated by weak density in $|F_o| - |F_c|(\phi_c)$ calculations (*18*), and forms only a single long hydrogen bond with O2 of P_N of NADH (3.2 Å). Hence, the net disruption of two hydrogen bonds near the pyrophosphate moiety of NADH which could account for a loss of 2 to 3 kcal/mol of binding energy and result in the mutant's fivefold reduced affinity for NADH. Notably, the side chain of Ile^{16}, which is replaced by Thr in an isoniazid-resistant clinical strain of *M. tuberculosis* (*5*, *8*), is also contained in the NADH-binding cleft and is in close proximity to the adenine ribose of NADH. It is likely that the substitution of the alkyl chain of Ile^{16} by a hydroxyl group also perturbs the hydrogen-bonding pattern of the cofactor binding site, leading to differences in NADH binding.

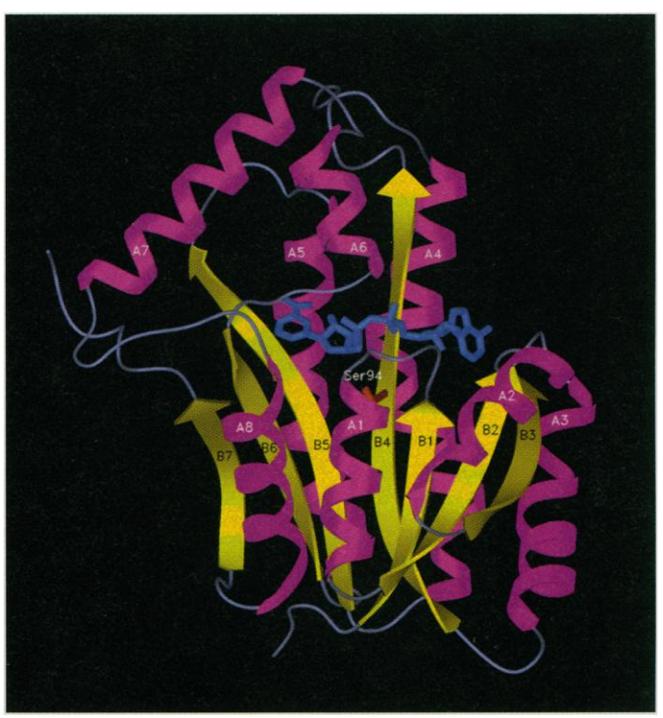

Fig. 1. Schematic ribbon drawing of InhA complexed with one NADH molecule. Secondary structure elements are labeled. The NADH binding fold can be further subdivided into two sections, the first formed by residues 2 to 54 and consisting of B1, A1, B2, and A2. Strand B3 is the crossover connection to the second part of the fold, formed by residues 57 to 192 and consisting of A3, B4 (a 14-residue β strand), A4, B5, A5 (a 21-residue α helix), and B6. Helices A6 and A7, together with the COOH-termini of β sheets B4 and B5 and the NH_2-termini of α helices A4 and A5, compose the "back" of the InhA chair. The last two structural elements in the fold, β sheet B7 and α helix A8, are part of the "legs" of InhA. NADH is shown as a smooth joint model in blue. Ser^{94} is shown in orange. The image was computed with the program SETOR (*25*).

Table 1. Kinetic parameters for wild-type and S94A mutant InhA proteins measured by following NADH oxidation at 340 nm with a Uvikon 93310 spectrophotometer (Kontron Instruments). All reactions were done in 30 mM Pipes buffer (pH 6.8) at 25°C. Standard reactions for the determination of the K_m of NADH contained 10 μM 2-*trans*-octenoyl-ACP, variable NADH (10 to 40 μM), and 7.5 nM InhA. Standard reactions for the determination of the maximum velocity and K_m for 2-*trans*-octenoyl-ACP contained variable 2-*trans*-octenoyl-ACP (4 to 25 μM), 100 μM NADH, and 7.5 nM InhA.

Enzyme	K_m (μM)		V_{max} (μmol min^{-1} mg^{-1})
	2-*trans*-octenoyl-ACP	NADH	
Wild-type	2 ± 1	8 ± 0	2.2 ± 0.4
S94A	3 ± 1	38 ± 2	3.1 ± 0.6

Table 2. Phasing statistics for InhA from *M. tuberculosis*. $R_{iso} = 100(\Sigma_{\vec{h}}|I_{PH}(\vec{h}) - I_P(\vec{h})|\Sigma_{\vec{h}}|I_{PH}(\vec{h}) + I_P(\vec{h})|)$, where I_{PH} and I_P are derivative and native intensities, respectively. Phasing power = $|\langle F(\vec{h})\rangle|/E$, where $\langle F(\vec{h})\rangle$ and E are average structure factor and lack of closure error, respectively. $R_{merge} = 100\ (\Sigma_{\vec{h}}\Sigma_i|\langle I(\vec{h}_i)\rangle - I(\vec{h}_i)|/\Sigma_{\vec{h}}\Sigma_i I(\vec{h}_i))$, where $\langle I(\vec{h}_i)\rangle$ is the average of symmetry equivalents.

Data set	Number of unique reflections	Extent of diffraction (Å)	R_{merge} (%)	R_{iso} (%)	Number of sites	Phasing power	Completeness (%)
Wild-type enzyme	18462	2.2	9.6	–	–	–	81.0
$Hg(C_2H_3O_2)_2$	21915	2.5	14.3	10.6	1	1.55	83.0
PCMPS	22261	2.5	13.9	10.7	4	1.60	84.5
S94A enzyme	9044	2.7	10.1	–	–	–	76.5

These kinetic and structural studies suggest one possible molecular mechanism of resistance to isoniazid. In the *E. coli* EnvM system (*11*), NADH or NAD^+ is required for binding of diazaborine, which then inhibits catalysis. $Gly^{93} \rightarrow Ser^{93}$ (G93S), the mutation in EnvM that confers diazaborine resistance, reduces enzyme affinity for the nucleotide and consequently for diazaborine. This leads to the development of a diazaborine-resistant phenotype. For the InhA system, we propose that the decrease in NADH binding affinity, caused by a perturbation of the hydrogen-bonding network in the S94A InhA and possibly I16T InhA active sites, may have a direct effect on the subsequent binding of the active form of isoniazid. This could be accomplished either by the preformation of a nucleotide-inhibitor complex or by a conformational change in the enzyme active site upon NADH binding, which affects the substrate binding site. In this scenario, the resulting decrease in the affinity of the mutant for the active form of isoniazid would underlie the development of drug resistance. Knowledge of the biochemical and structural features of InhA provides a framework for understanding how mutations affect drug binding to enoyl-ACP reductase and will facilitate rational design of new antitubercular drugs.

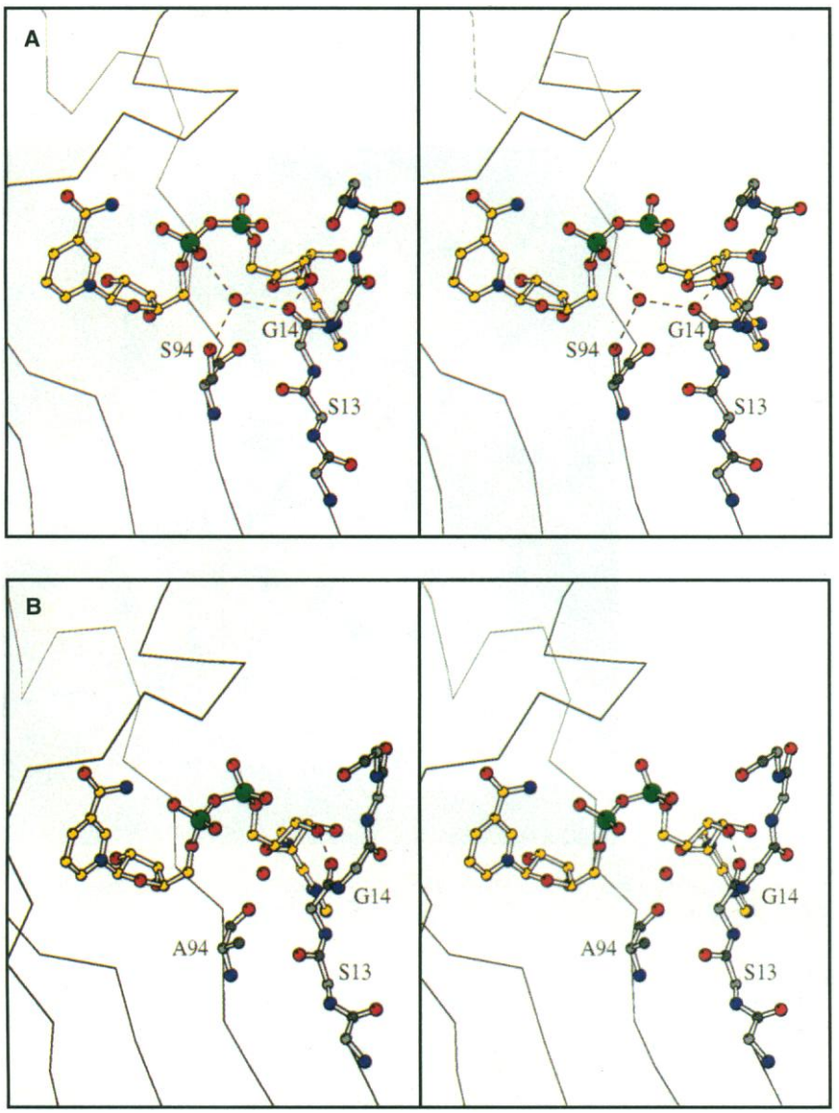

Fig. 2. Stereo view of the atoms in the binding site of NADH in wild-type (**A**) and mutant (**B**) structures. Only the regions proposed to be involved in acquisition of isoniazid resistance are shown, for clarity. Nitrogen atoms are depicted in blue, oxygen in red, and phosphate in green. Carbon atoms of NADH are yellow, and protein carbon atoms are gray. Only the backbones of residues 12 to 16 are shown, but all atoms are displayed in residue 94. Ramachandran angles for Gly^{14} in the wild-type structure are Φ = 84.1° and Ψ = 40.8°; in the mutant they are Φ = 117.4° and Ψ = −74.5°. The images were generated with the program MOLSCRIPT (*26*).

REFERENCES AND NOTES

1. G. Middlebrook, *Am. Rev. Tuberc. Pulm. Dis.* **65**, 765 (1952).
2. D. Snider and W. Roper, *N. Engl. J. Med.* **326**, 703 (1992).
3. K. Takayama, L. Wang, H. L. David, *Antimicrob. Agents Chemother.* **2**, 29 (1972); F. G. Winder, in *The Biology of Mycobacteria*, C. Ratledge and J. Stanford, Eds. (Academic Press, London, 1982), vol. 1, pp. 354–438; A. Quémard, C. Lacave, G. Laneelle, *Antimicrob. Agents Chemother.* **35**, 1035 (1991).
4. Y. Zhang, B. Heym, B. Allen, D. Young, S. Cole, *Nature* **358**, 591 (1992); M. Stoeckle *et al.*, *J. Infect. Dis.* **168**, 1063 (1993).
5. B. Heym *et al.*, *Lancet* **344**, 293 (1994).
6. K. Johnsson and P. G. Schultz, *J. Am. Chem. Soc.* **116**, 7425 (1994).
7. A. Banerjee *et al.*, *Science* **263**, 227 (1994).
8. V. Kapur *et al.*, *Arch. Pathol. Lab. Med.* **119**, 131 (1995).
9. H. Bergler, G. Hogenauer, F. Turnowsky, *J. Gen. Microbiol.* **138**, 2093 (1992).
10. M. A. Grassberger, F. Turnowsky, J. Hildebrand, *J. Med. Chem.* **27**, 947 (1984).
11. H. Bergler *et al.*, *J. Biol. Chem.* **269**, 5493 (1994).
12. InhA has a mass of 28,368 daltons, which is in agreement with the mass predicted from the gene sequence (28,547; the first Met is cleaved by *Escherichia coli* and the second amino acid is Ala instead of Thr).
13. A. R. Slabas *et al.*, *Biochim. Biophys. Acta* **877**, 271 (1986).
14. A. Quémard, J. C. Sacchettini, A. Dessen, W. R. Jacobs Jr., J. S. Blanchard, in preparation.
15. The InhA-NADH complex was crystallized by the hanging drop vapor diffusion method. The protein solution [3 μl containing enzyme (13 mg/ml) in a 1:2 ratio with NADH] was mixed with precipitant solution [3 μl containing 50 mM Hepes (pH 7.2), 8 to 12% methyl pentane diol (MPD), and 50 mM sodium citrate (pH 6.5)] on a silanized cover slip that was inverted and sealed above the precipitant solution (700 μl). Two heavy-atom derivatives [*p*-chloromercuriphenylsulfonate (PCMPS) and $Hg(C_2H_3O_2)$] were used to solve the wild-type structure. The mercury acetate derivative was obtained by soaking of a native crystal (containing NADH) overnight in 1 mM $Hg(C_2H_3O_2)$ and 10% MPD, 50 mM Hepes (pH 7.2), and 50 mM sodium citrate (pH 6.5). The PCMPS derivative was obtained by prereaction of the protein [13 mg/ml in 10 mM Hepes (pH 7.2) in a 1:2 ratio with NADH] with 10 mM PCMPS for ~30 min at 19°C and then crystallization of the complex under the same conditions that yielded native crystals. All data sets were collected on a Siemens multiwire area detector, with the use of a Rigaku RU-200 rotating anode x-ray source operating at 55 kV and 85 mA. Data were reduced with the use of the Siemens package XENGEN (*19*) on a Silicon Graphics Iris computer. Heavy-atom derivative parameters were refined with PHASES (*20*) and XtalView (*21*). The initial electron density map was submitted to solvent flattening, phase extension, and histogram matching (*20, 22*). A partial polyalanine model was built with the use of the program TOM (*23*), displayed on an Iris Graphics workstation, and refined by means of molecular dynamics and energy minimization (*18, 24*). Subsequent calculation of combined maps (maps obtained combining model-based and MIR phases) permitted tracing of the complete model and incorporation of the complete amino acid sequence, as well as introduction of the NADH molecule. The refined positions of the heavy metals were also used to confirm the modeled phases. The final model included all 268 residues and 67 water molecules, yielding a final *R* factor of 19.6%, with root mean square (rms) values of 0.020 Å and 2.1° in bond lengths and bond angles, respectively.
16. S94A InhA was purified in the same fashion and crystallized under the same conditions as the wild-type enzyme. Rigid body refinement of the monomer with X-PLOR (*18*) yielded an *R* factor of 24% for the x-ray diffraction data between 12 and 3.5 Å. Several cycles of TNT (*24*) and manual model building subsequently decreased the *R* factor to a final value of 19.3% for data up to 2.7 Å. Simulated annealing

electron density omit maps encompassing the NADH binding site were used during refinement of the coordinates. The final model contained all 268 residues and 48 solvent molecules, with rms values of 0.021 Å and 2.3° in bond lengths and bond angles, respectively.
17. M. G. Rossmann, A. Liljas, C. Granden, L. Banaszak, *The Enzymes*, P. Boyer, Ed. (Academic Press, New York, ed. 3, 1975), vol. 11A, pp. 61–102.
18. A. T. Brünger, J. Kuriyan, M. Karplus, *Science* **235**, 458 (1987); A. T. Brünger, *X-PLOR Version 3.0 Manual* (Yale Univ. Press, New Haven, CT, 1992).
19. A. J. Howard, *A Guide to Data Reduction for the Nicolet Imaging Proportional Counter: The XENGEN System* (Genex Corporation, Gaithersburg, MD, 1986).
20. W. Furey and W. Swaminathan, *Am. Crystallogr. Assoc. Program Abstr.* **18**, 73 (1990).
21. D. McRee, in *Practical Protein Crystallography* (Academic Press, New York, 1993), pp. 303–374.
22. B.-C. Wang, *Methods Enzymol.* **115**, 90 (1985).
23. T. A. Jones, *ibid.*, p. 157.
24. D. E. Tronrud, L. F. Ten Eyck, B. W. Matthews, *Acta Crystallogr. Sect. A.* **43**, 489 (1988).
25. S. V. Evans, *J. Mol. Graphics* **11**, 134 (1993).
26. P. J. Kraulis, *J. Appl. Crystallogr.* **24**, 946 (1991).
27. Supported by NIH grants AI33696, AI30189, and AI36849, and by a postdoctoral fellowship (to A.D.) from the Heiser Foundation for Research in Leprosy and Tuberculosis. Coordinates will be deposited in the Brookhaven Protein Data Bank.

8 October 1994; accepted 6 January 1995

Evidence from 18S Ribosomal DNA That the Lophophorates Are Protostome Animals

Kenneth M. Halanych, John D. Bacheller, Anna Marie A. Aguinaldo, Stephanie M. Liva, David M. Hillis, James A. Lake

The suspension-feeding metazoan subkingdom Lophophorata exhibits characteristics of both deuterostomes and protostomes. Because the morphology and embryology of lophophorates are phylogenetically ambiguous, their origin is a major unsolved problem of metazoan phylogenetics. The complete 18S ribosomal DNA sequences of all three lophophorate phyla were obtained and analyzed to clarify the phylogenetic relationships of this subkingdom. Sequence analyses show that lophophorates are protostomes closely related to mollusks and annelids. This conclusion deviates from the commonly held view of deuterostome affinity.

Understanding the phylogenetic affinities of the lophophorates (brachiopods, bryozoans, and phoronid worms) is a major unresolved issue of metazoan phylogenetics. The lophophorate taxa are thought to constitute a monophyletic subkingdom, superphylum, or phylum (*1*, *2*) because they possess a similar suspension-feeding apparatus, the lophophore [a ciliated ring of tentacles, invaded by the mesocoelomic cavity, that surrounds the mouth but not the anus (*1*, *3*)]. Because of their unusual morphologies, the phylogenetic relationships of lophophorates may provide important clues about the evolution of morphology and development in protostome and deuterostome animals.

Many phylogenetic hypotheses have been proposed for the lophophorates. They have been classified as protostomes, as deuterostomes, as members of both groups, or as an independent metazoan lineage. Earlier researchers often allied lophophorates with protostome taxa on the basis of the presence in both lophophorates and deuterostomes of chitin, the lack of sialic acids, and several embryological features (*1*, *4*). Analyses of incomplete 18S ribosomal DNA (rDNA) data from an inarticulate brachiopod are also consistent with protostome affinities (*5*). However, the most recent reanalyses of embryology (including blastopore fate, coelom formation, and cleavage patterns) (*6*, *7*) and morphology have led most researchers to believe that lophophorates are basal deuterostomes (*1*, *2*, *4*). The deuterostome hypothesis has been supported by recent phylogenetic analyses of morphology and embryology (*8*, *9*) on the basis of the presence in both lophophorates and deuterostomes of a tripartite coelomic arrangement, a modified radial cleavage, a ciliary food-collecting system that captures particles upstream relative to the ciliary beat, a lophophore-like apparatus (also present in echinoderms and pterobranch hemichordates), and a U-shaped adult digestive tract.

We used molecular sequence analyses to circumvent several problems associated with the interpretation of morphological and embryological characters. To reconstruct the evolution of the lophophorates, we sequenced complete 18S rDNAs from representative lophophorate taxa, aligned them with existing data from other metazoan taxa (*10*), and analyzed them with standard phylogenetic techniques. We chose rDNA to examine metazoan origins because it has evolved at an appropriate rate (*5*, *11*). *Anemonia sulcata* (an anthozoan) and *Tripedalia cystophora* (a scyphozoan) were used as the outgroups to triploblastic animals, which are thought to be monophyletic on the basis of morphological and molecular data (*12*).

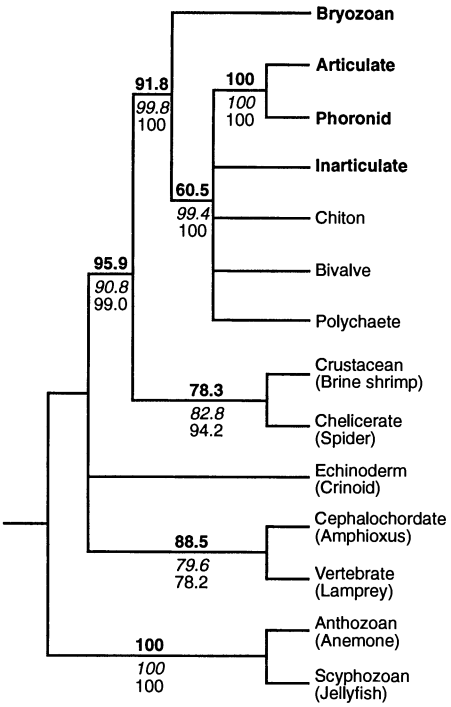

Fig. 1. Phylogenetic analyses of 18S rDNA sequence data to determine the position of the lophophorate metazoans (*10*). Lophophorate taxa are indicated in boldface. The consensus topology shown here is a consensus of the best trees given by four different methods: maximum likelihood analysis, bootstrap analysis of parsimony, bootstrap analysis of neighbor-joining with maximum likelihood estimates of Kimura two-parameter distances, and bootstrap analysis of paralinear distances. The numbers next to the nodes represent the bootstrap proportions (out of 500 iterations) for the parsimony analysis (top, bold numbers), the neighbor-joining analysis (middle, italic numbers), and the paralinear distance analysis (bottom, roman numbers).

The consensus tree derived from our reconstructions is shown in Fig. 1. In all of the reconstructions (including likelihood, parsimony, and distance methods), the lophophorate taxa clustered within the protostomate clade along with the annelid and molluscan taxa (*13*). The clade containing the lophophorates, the annelids, and the mollusks is present in 91.8, 99.8, and 100% of the trees derived from bootstrap reconstructions of data obtained through maxi-

K. M. Halanych, Department of Zoology, University of Texas, Austin, TX 78712, USA, and Molecular Biology Institute and Biology Department, University of California, Los Angeles, CA 90024, USA.
J. D. Bacheller, A. A. Aguinaldo, S. M. Liva, J. A. Lake, Molecular Biology Institute and Biology Department, University of California, Los Angeles, CA 90024, USA.
D. M. Hillis, Department of Zoology, University of Texas, Austin, TX 78712, USA.